Hindawi Publishing Corporation
Mathematical Problems in Engineering
Volume 2016, Article ID 2865195, 18 pages
http://dx.doi.org/10.1155/2016/2865195

Research Article

Analyzing Chaos Systems and Fine Spectrum Sensing Using Detrended Fluctuation Analysis Algorithm

Javier S. González-Salas,[1] Modar S. Shbat,[2] Francisco C. Ordaz-Salazar,[2] and Jorge Simón[3]

[1]*Mathematical Department, Polytechnic University of San Luis Potosi, Urbano Villalón 500, 78363 San Luis Potosí, SLP, Mexico*
[2]*Telematics Engineering Department, Polytechnic University of San Luis Potosí, Urbano Villalón 500, 78363 San Luis Potosí, SLP, Mexico*
[3]*Centro de Investigación y Desarrollo en Telecomunicaciones Espaciales de Ingeniería Eléctrica, Universidad Autónoma de Zacatecas, 801 Ramón López Velarde, 98000 Zacatecas, ZAC, Mexico*

Correspondence should be addressed to Modar S. Shbat; modar.shbat@upslp.edu.mx

Received 15 January 2016; Revised 6 April 2016; Accepted 7 April 2016

Academic Editor: Oleg V. Gendelman

A numerical study that uses detrended fluctuation analysis (DFA) algorithm of time series obtained from linear and nonlinear dynamical systems is presented. The DFA algorithm behavior toward periodic and chaotic signals is investigated and the effect of the time scale under analysis is discussed. The displayed results prove that the DFA algorithm response is invariant (stable performance) to initial condition and chaotic system parameters. An initial idea of DFA algorithm implementation for fine spectrum sensing (SS) is proposed under two-stage spectrum sensor approach with test statistics based on the scaling exponent value. The outcomes demonstrate a promising new SS technique that can alleviate several imperfections such as noise power uncertainty and spatial correlation between the adjacent antenna array elements.

1. Introduction

Detrended fluctuation analysis (DFA) is an effective numerical tool used to measure the persistency (or antipersistency) of data series with nonstationarities. DFA characterizes their complex behavior by identifying the long-range power law correlations. The DFA algorithm has several advantages over the conventional analysis methods such as power spectrum and correlation analysis owing to that it avoids false detections originated from artifacts of spurious or not precise measured observations from real systems. Besides, DFA is widely used to detect and/or characterize if a time series is random or not. DFA algorithm has been applied in different areas, for example, weather, economy, biology, meteorology, and climate [1, 2]. According to the new research trends, the DFA algorithm is implemented to analyze the WEB [3], to estimate synchrophasor measurements [4], to analyze oil reservoirs [5], to study volcano seismicity [6], and to study earthquakes [7].

Chaotic systems (CSs) are nonlinear deterministic systems that generate random and unpredictable time series which have statistical properties similar to random processes [8]. CSs generate time series with chaotic behavior that can be observed in data from observations [9]. It is important to study the effects of the DFA algorithm on the chaotic series because many noisy data observations are extracted from physical, biological, and social systems. These systems exhibit scale-invariant features and contain hidden long-range power law correlations that can be detected using DFA algorithm and can provide interesting and useful information about the structure and evolution of any dynamic system. There are few articles that can be categorized in this research direction, like in [10] where the authors studied and characterized time series from a Chua System.

The DFA algorithm is investigated in many research articles [11, 12] and applied to solve some problems in many engineering areas. Furthermore, the DFA algorithm is compared with other well-known and effective algorithms such

as power spectral density analysis [13], correlation dimension [14], and wavelet [15].

A very big set of tools have been developed to analyze the deterministic and predictable signals such as periodic, transient, and stochastic signals. Chaotic signals are deterministic signals with unpredictable related time series. In many cases, chaotic signals appear like noise (deterministic but not predictable) and could be analyzed using conventional stochastic tools. In [16], a numerical study of the DFA algorithm response under data series from discrete chaotic systems is presented. It is shown that the DFA algorithm detects, in low scale intervals, the short range correlations in chaotic data series that are very similar to noise. The last characteristic can have important applications in telecommunication systems. The moving DFA (MDFA) algorithm in [17] could detect time-instants of abrupt changes in dynamic structures where the analyzed chaotic system parameters are changed. The MDFA performance is independent of the length of subseries and has a perfect capability to resist the effects of noise. Unfortunately, no direct applications were mentioned in [16, 17] for the presented work. Besides, there is no statistical analysis about the robustness of the DFA algorithm under the variation of the parameters and the initial conditions of the chaotic systems. The missed statistical analysis is presented in this paper (the initial conditions of chaotic data series from real systems are usually unknown).

An interesting analysis is presented by [18] in the field of signal processing when the DFA algorithm is employed as a denoising technique. The DFA algorithm in [18] is used to select the band limited intrinsic mode functions (IMFs) of the broken down noisy signal and to define the relevant modes in order to construct the filtered signal. The proposed method is valid only under the use of variational mode decomposition (VMD) and for white Gaussian noise. In [19], the authors proposed a metric based on DFA to define a robust threshold that determines which oscillations (called IMFs) are noise components or noise free signal components under empirical mode decomposition (EMD). The presented results are promising and significant around 0 dB range of signal-to-noise ratio (SNR), limited SNR region, and for the white Gaussian noise as in the case of [18]. The multifractal DFA (MF-DFA) algorithm is proposed as a detection approach of ionospheric irregularities for global navigation satellite system (GNSS) receivers [20] (GNSS signal detection). The MF-DFA was combined with complementary ensemble empirical mode decomposition (CEEMD) to analyze nonlinear and nonstationary signals (positive and negative white noises are added to the data). This combination increases the complexity of the detection technique and, in some cases, leads to generate a different number of modes that contain new components not related to the signal at the receiver input (the inclusion of white noise with inappropriate amplitudes).

Since many physical signals are noisy and heterogeneous and exhibit different types of nonstationarities which can affect the correlation properties of these signals and based on the previous review of the related literature, it is evident that the DFA algorithm can be applied in different engineering areas and helps to alleviate some specific problems.

In this paper, with the purpose to extend and observe the DFA algorithm response to data from well-known chaotic systems, the Lorenz, the Rossler, and multistable systems are considered. The main properties of the DFA algorithm that could be used to characterize nonlinear systems time series are presented. The output of this analysis leads us to propose the employment of the DFA algorithm in new engineering area, namely, spectrum sensing in cognitive radio (CR) systems.

It is evidently confirmed that the available licensed spectrum is not efficiently and fully utilized by the related wireless technologies in time and spatial domains. Cognitive radio (CR) introduces a futuristic concept that helps to dynamically use the spectrum in an opportunistic manner. The spectrum sensing (SS) in CR defines accurately the vacant frequency bands (frequency holes) by detecting the existence of the primary user (PU) signals in the spectrum of interest. Up to this day, plenty of SS techniques and approaches were presented under different initial practical conditions such as low signal-to-noise ratio (SNR), spatially correlated multiple antennas, and noise power uncertainty. In [21], a wide review of SS algorithms and some other important topics in CR are discussed.

Owing to its simplicity when no prior knowledge about the PU signal is required, the energy detector (ED) is commonly used as a coarse spectrum sensor [22]. The ED suffers from performance degradation at low SNR with noise variance uncertainty (SNR wall problem) and spatial correlation of multiple antennas (between the antenna array elements) [23, 24].

The two stages sensing architecture that combines two detectors was proposed by the IEEE 802.22 working group (standards). In this work, we consider two-stage SS scheme for CR systems. The coarse (fast, several tens of micro seconds) sensing stage is performed by the ED and the fine sensing (several tens of milliseconds) stage is based on the DFA algorithm. The topology of two stages SS is proposed with the purpose to maximize the probability of detection under practical imperfections like noise power uncertainty and spatially correlated antenna array elements. The main motivation of using the DFA algorithm for fine SS is that DFA shares with ED the same property of no information about the PU signal is needed and the SS can be effectively performed based on the input data samples. The final decision about the PU signal presence or absence is made by combining the decisions of the two stages using "OR" rule (other types of rules can be applied such as "And" or "Majority"). The implementation of DFA algorithm for fine SS demonstrates promising results and gives insight about the possibility of using DFA in CR systems as a new signal detection scheme and also for other applications in telecommunication and sensor systems. All the presented numerical results in this paper are generated using MATLAB.

The remainder of this paper is organized as follows. Section 2 contains the DFA algorithm main steps. In Section 3, the DFA is applied in periodic systems (sinusoidal signals) under different parameter values. In Section 4, various numerical experiments are performed for three different chaotic systems, namely, Lorenz, Rossler, and the

Step 1. Random walk calculation:
for $i = 1 : N$ $(1 \le i \le N)$
$\langle s \rangle = (1/N) \sum_{i=1}^{N} s(i)$ (the mean of the data series);
$y(i) = \sum_{k=1}^{i} [s(k) - \langle s \rangle]$;
end for
Step 2. Using the interval size n, $y(i)$ is divided to $\lfloor N/n \rfloor$ intervals
Step 3. **for** $j = 1 : N/n$
The fitting process is performed using polynomial function of order $l \Rightarrow y_l(i)$;
end for
Step 4. **for** $j = 1 : N/n$
for $i = 1 : n$
$Y_l(i) = y(i) - y_l(i)$; (detrended fluctuation signal)
end for
end for
Step 5. Root mean square (rms) calculation:
for $i = 1 : N$ $(1 \le i \le N)$

$$F_l(n) = \sqrt{\frac{1}{N} \sum_{i=1}^{N} \left[Y_l(i)\right]^2};$$

end for
Step 6. Finding the relation between the fluctuation and the scale:
for $n = 4 : N/4$ $(4 \le n \le N/4)$
repeat the steps from 1 to 5 (1~5)
end for
The power law relation: $F_l(n) \sim n^{\alpha}$ where

$$\alpha = \frac{\log_p(F_l(n))}{\log_p(n)}$$

Algorithm 1: The DFA algorithm steps.

multistable system. The DFA algorithm implementation for fine spectrum sensing is presented in Section 5. Finally, the conclusion remarks are given in Section 6.

2. DFA Main Steps

Define $s(i)$, the data series to be analyzed by DFA where $1 \le i \le N$ and N is the data series size. The DFA algorithm can be applied using the following standard steps:

(i) Calculate the random walk of the data series $s(i)$ using

$$y(i) = \sum_{k=1}^{i} [s(k) - \langle s \rangle], \tag{1}$$

where $\langle s \rangle$ is the mean of the data series $s(i)$ given by

$$\langle s \rangle = \frac{1}{N} \sum_{i=1}^{N} s(i). \tag{2}$$

(ii) The series $y(i)$ is divided into $\lfloor N/n \rfloor$ data intervals of equal size n where the notation $\lfloor \cdot \rfloor$ represents the floor function.

(iii) In each data interval, the data is fitted by using a polynomial function of order l to obtain $y_l(i)$ which is called the local trend (order-l DFA). In previous studies [25–27], the value $l = 1$ is commonly used, that is, the linear detrended fluctuation of the signal. Nevertheless, any polynomial function of grade $l \neq 1$ could be used for the data fitting step.

(iv) The integrated signal $y(i)$ is detrended by subtracting the local trend $y_l(i)$ in each data interval generating the detrended fluctuation signal:

$$Y_l(i) = y(i) - y_l(i). \tag{3}$$

(v) For an interval size n, the root mean square (rms) of the detrended fluctuation signal is calculated:

$$F_l(n) = \sqrt{\frac{1}{N} \sum_{i=1}^{N} \left[Y_l(i)\right]^2}. \tag{4}$$

(vi) In order to find the relation between the scaling exponent and the data fluctuation, the previous steps are repeated for different data interval sizes $4 \le n \le N/4$. The power law relation

$$F_l(n) \sim n^{\alpha} \tag{5}$$

indicates the scaling presence where α is the scaling or the correlation exponent. Algorithm 1 gives a brief summary about the main DFA steps.

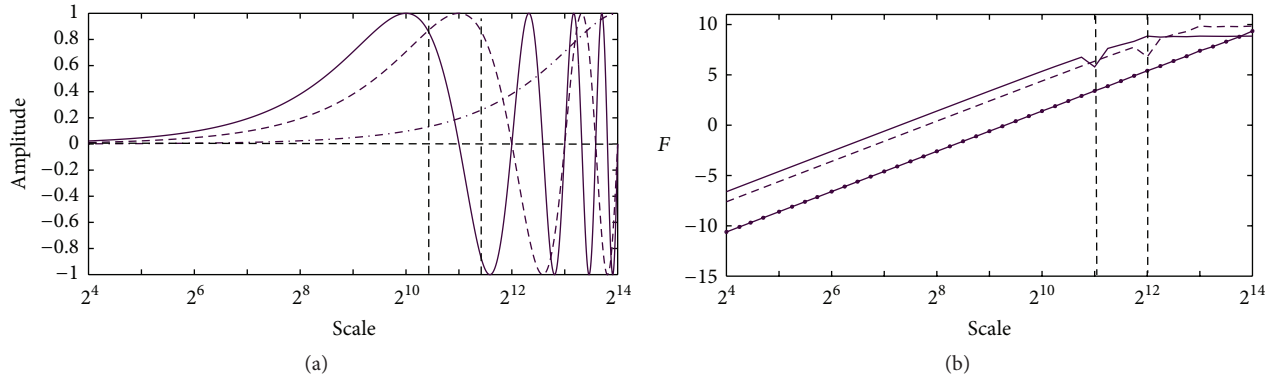

Figure 1: (a) The sinusoidal signal amplitude as a function of the scale (for the cases: $f = 1$ dashed-dotted line, $f = 8$ dashed line, and $f = 16$ continuous line), (b) DFA analysis for the sinusoidal signal ($f = 1$ points line, $f = 8$ dashed line, and $f = 16$ continuous line).

In this paper, the polynomial functions of grade $l = 1$ are used. Thus, $F_1(n)$ is referred to as $F(n)$. The correlation properties of a signal are characterized based on the scaling exponent α. For the linear case ($l = 1$), if $\alpha = 0.5$, then the signal under analysis is uncorrelated (random process). In the case when $\alpha < 0.5$, the signal is anticorrelated, and for $\alpha > 0.5$ the signal contains positive correlations. The scaling exponent α can be determined using (5) as follows:

$$\alpha = \frac{\log_p (F(n))}{\log_p (n)}, \tag{6}$$

where p is a positive integer. The value of α is defined from the slope of the straight line that is adjusted from the points $(\log_p(F(n)), \log_p(n))$. For the presented numerical analysis in this paper, the value $p = 2$ is used.

3. Periodic (Sinusoidal) Signals

The DFA algorithm response to periodic signals by using sinusoidal sequences is investigated. The periodic signal used in this section is defined as:

$$s(t) = A \sin\left(2\pi f t + \varphi\right), \tag{7}$$

when the amplitude $A = 1$, the frequency $f = \{1, 8, 16\}$, and the phase $\varphi = 0$. Figure 1(a) shows the amplitude of the sinusoidal signal as a function of the time scale, and Figure 1(b) contains the respective F fluctuations. The slope of the graphs that correspond to the fluctuation of sinusoidal signals with frequencies $f = 8$ and $f = 16$ approaches zero at scale values equal to 2^{12} and 2^{13}, respectively. These values correspond to one period of their related sinusoidal signals. If one cycle or period of the sinusoidal signal with the slow frequency $f = 1$ (period $T_1 = 1$) has $2^{16} = 65536$ samples by cycle, then the period of the signal with $f = 16$ is equal to $T_{16} = 2^{16}/16 = 2^{16}/2^4 = 2^{12}$, and for the signal with $f = 8$ we have $T_8 = 2^{16}/8 = 2^{16}/2^3 = 2^{13}$. Thus, for sinusoidal signal, the DFA algorithm gives a saturation value of the scaling exponent $\alpha = 0$ which corresponds to a signal that oscillates between two values. The dents positioned at scale values 2^{11} and 2^{12} correspond to the time at which the signal flows from positive to negative values (see Figure 1(b)).

After analyzing the DFA algorithm for a periodic signal with only one harmonic component, a numerical analysis of the DFA response for signals with more harmonic components is conducted. Figure 2(a) shows the compound signal defined as $A_1 \sin(2\pi f_2 t) + A_2 \sin(2\pi f_{16} t)$ case at $A_1 = A_2 = 1$, $f_2 = 2$, and $f_{16} = 16$ (with periods $T_2 = 1/2$ and $T_{16} = 1/16$, resp.) under sampling time $t_s = 2^{-12}$. Furthermore, the respective DFA response is presented in Figure 2(b).

As shown in the previous case, the dents in Figure 2 are positioned at $(T_{16}/2)/t_s = 2^{12}/2^5 = 2^7$ and $(T_2/2)/t_s = 2^{12}/2^2 = 2^{10}$ that are placed at the instants where each sinusoidal signal crosses the horizontal axes towards the negative values. The case when the amplitudes of the sinusoidal signals are not equal ($A_1 \neq A_2$) is presented in Figure 2(c) when the component with the higher frequency $f = 16$ has greater amplitude $A_2 = 1$ in comparison with the amplitude of sinusoidal component with lower frequency. As the amplitude A_1 becomes smaller, the DFA algorithm does not detect the component $A_1 \sin(2\pi f_2 t)$. It is inferred that the fluctuation graphs F calculated with the small A_1 become horizontal when the period of the component $A_2 \sin(2\pi f_{16} t)$ is completed; that is, at the scale value $t_s^{-1}/16 = 2^{12}/2^4 = 2^8$. On the other hand, Figure 2(d) contains the DFA results for a constant $A_1 = 1$ and for $A_2 < A_1$. Analogous to the previous results, the DFA algorithm is not able to detect the component $A_2 \sin(2\pi f_{16} t)$. Besides, it is inferred that the deviation at the scale value 2^7 vanishes as A_2 becomes smaller.

4. Chaotic Signals

In this section, we are interested in processing time series of chaotic systems arising from differential equation that can be presented using the following form:

$$\frac{dX}{dt} = AX + G(X), \tag{8}$$

where $X = [x, y, z] \in \Re^k$ is the state variable (in our case $k = 3$), $G(X)$ is a function with domain and range space $\subset \Re^3$,

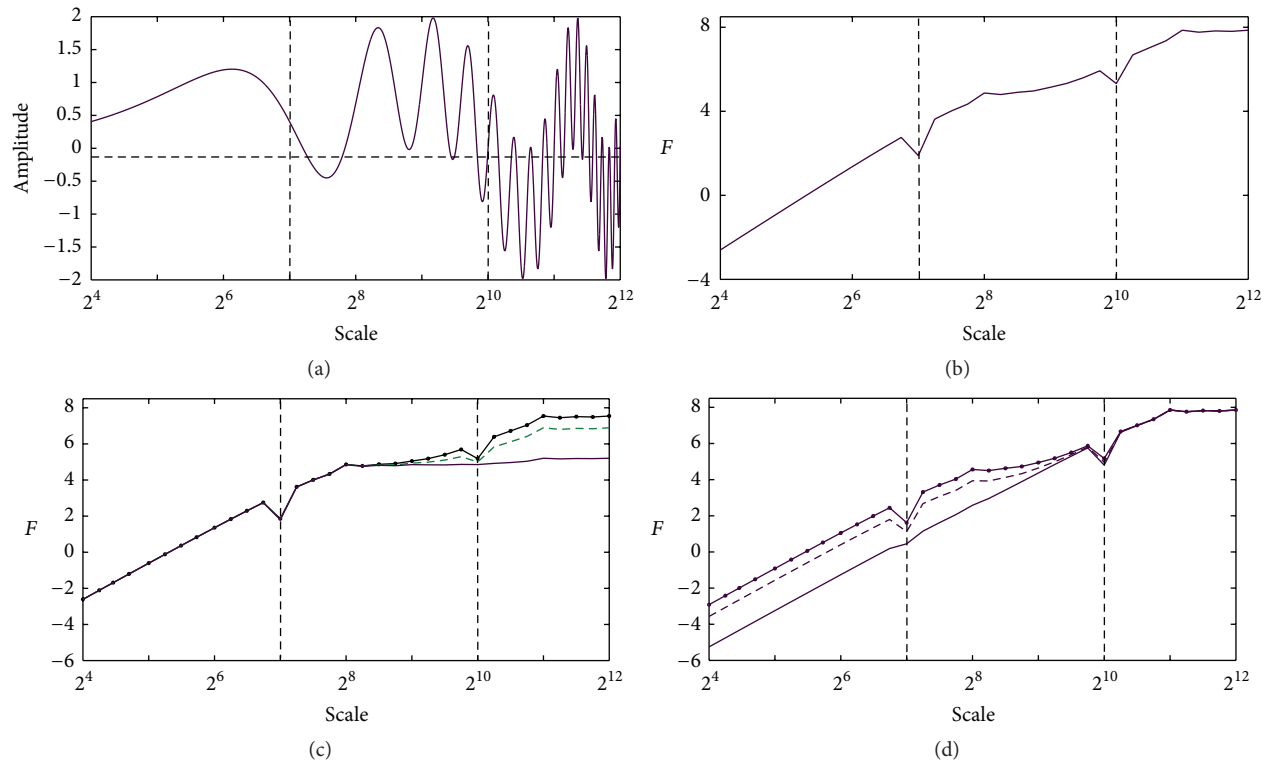

Figure 2: (a) The compound sinusoidal signal amplitude as a function of the scale. (b, c, d) The DFA analysis for the cases: $A_1 = A_2 = 1$, $A_1 \neq A_2$, and $A_2 < A_1$, respectively.

and $A = [\alpha_{ij}] \in \Re^{3\times 3}$ denotes a linear operator. Two main cases are analyzed, namely,

(i) when $G(\cdot)$ is a nonlinear function;

(ii) when $G(\cdot)$ is a piecewise linear function.

The DFA algorithm numerical results are presented for time series of differential systems (8) when the related initial conditions are varied and for various parameter values (such that their orbits conserve a chaotic regime).

4.1. Lorenz System. The Lorenz system is a very well-known third-order chaotic system [28] and can be defined as follows:

$$A = \begin{bmatrix} -\sigma & \sigma & 0 \\ \rho & -1 & 0 \\ 0 & 0 & -\beta \end{bmatrix}, \qquad G(X) = \begin{bmatrix} 0 \\ -xy \\ yz \end{bmatrix}, \tag{9}$$

where x, y, and z make up the system state; σ, ρ, and β are the system parameters. Figures 3(a), 3(b), and 3(c) show the time series of the Lorenz system's state variables x, y, and z, respectively. To generate these time series, the fourth-order Runge-Kutta method is used with a step of 0.01 (this step size is used for all numerical experiments related to Lorenz system) and main parameter values $\sigma = 10.0$, $\rho = 28.0$, and $\beta = 2.66$. Figure 3(d) presents the DFA response for these time series. In this figure it is observed that the fluctuations for x and y are very similar and that the general behavior of the fluctuation has three states, two fixed states and a transition between them:

(i) The first fixed fluctuation state for the scale interval $2^{4.75} \leq \text{scale} < 2^{7}$ where the values of the scaling exponent are 1.57, 1.437, and 1.437 for the variables x, y, and z, respectively.

(ii) The second fixed fluctuation state for the scale interval $2^{7.5} \leq \text{scale} < 2^{12}$ where the corresponding scaling exponent values are approximately 0.75, 0.72, and 0.3 for x, y, and z, respectively.

(iii) The transition between the previous states.

It is well known that the chaotic systems are very sensitive to initial conditions. In other words, regardless of the closeness to the initial conditions, the chaotic systems orbits will flow for different ways. To describe the response of the DFA algorithm under different initial conditions, a set of time series is considered with the same parameter values (σ, ρ, β) and initial conditions $X(0) = (k_1, k_2, 10)$ where the initial values k_1 and k_2 are taken in the intervals $-25 \leq k_1 \leq 25$ and $5 \leq k_2 \leq 40$ with steps 1.0 ($k_1, k_2 \in \mathrm{Z}$). In Figures 4(a) and 4(b) corresponding to DFA graphs from time series of variables x and y, it can be seen that the areas covered by their respective set of curves are very similar. To define the way

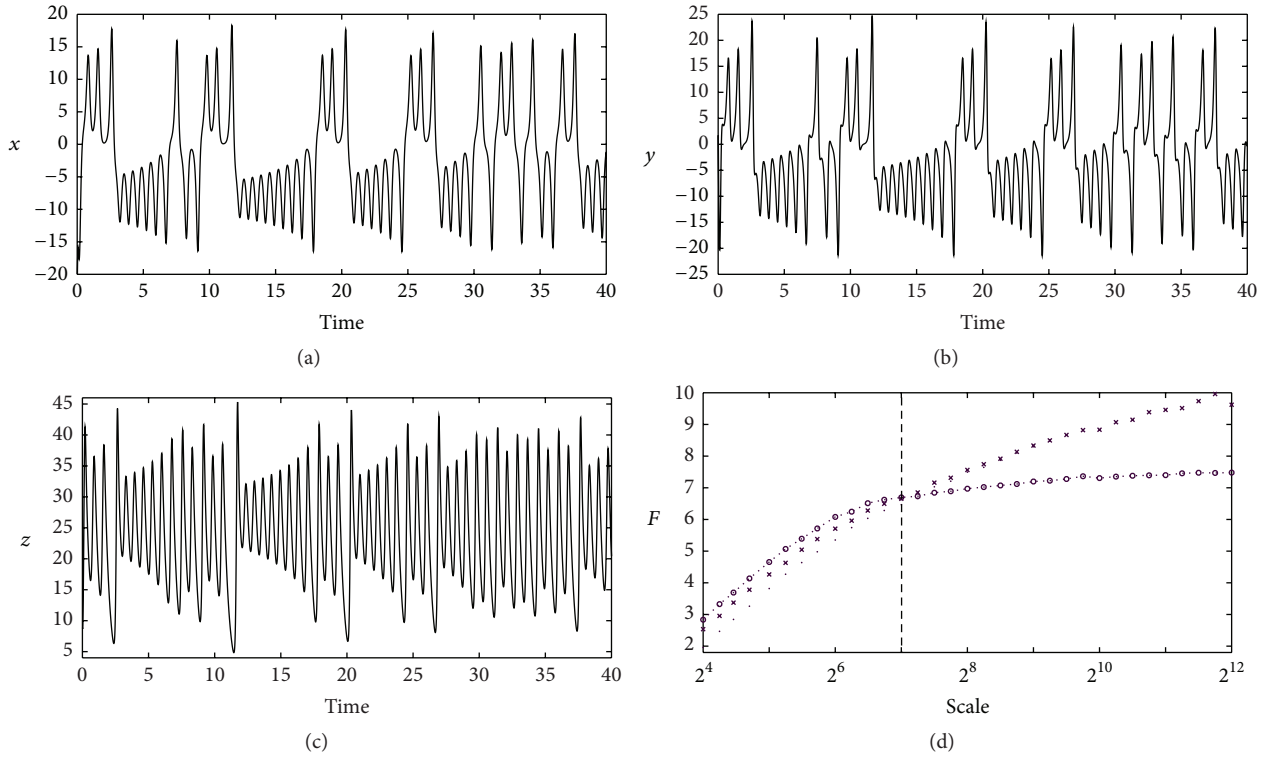

FIGURE 3: Lorenz time series: (a) the variable x, (b) the variable y, (c) the variable z, and (d) the fluctuation graphs for x, y, z (dots, crosses, and dotted line with circles, resp.).

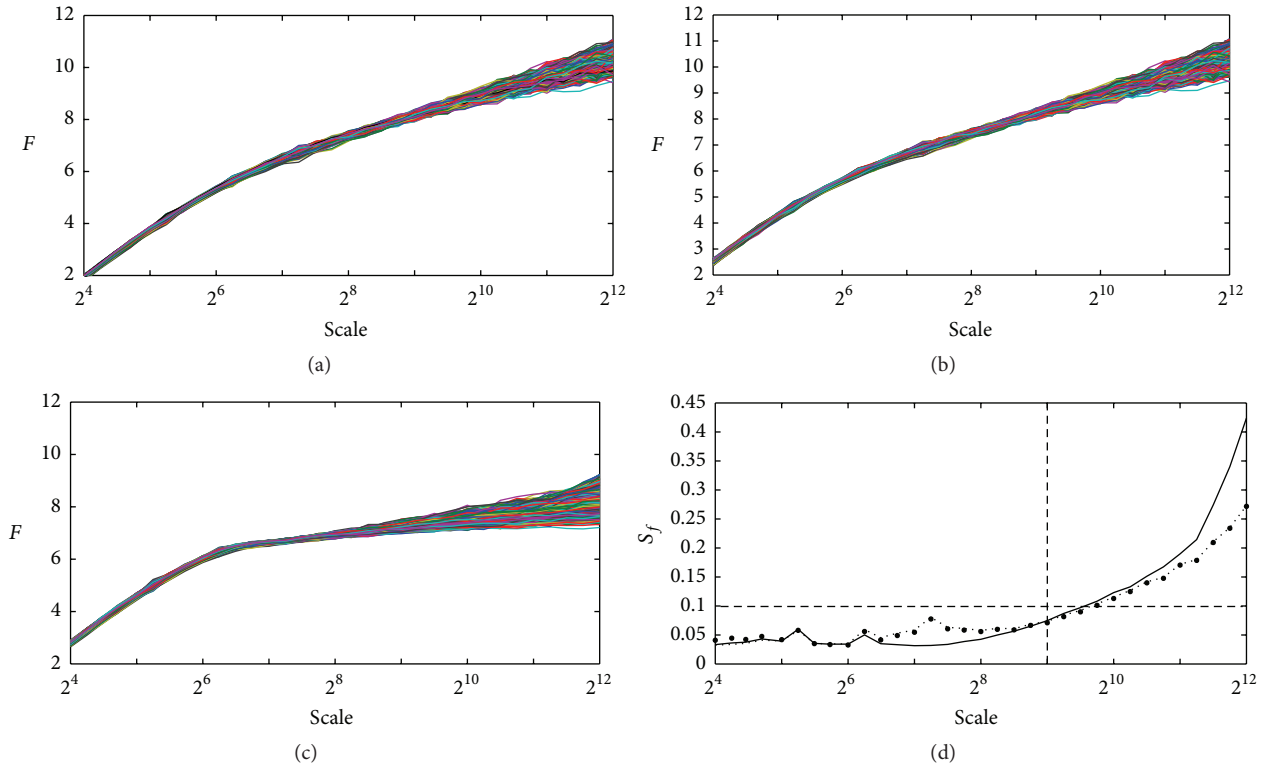

FIGURE 4: The DFA analysis of the Lorenz time series under different conditions for the variables: (a) x, (b) y, and (c) z and the related standard deviation of the DFA graphs in (a) dotted line, (b) circles line, and (c) continuous line.

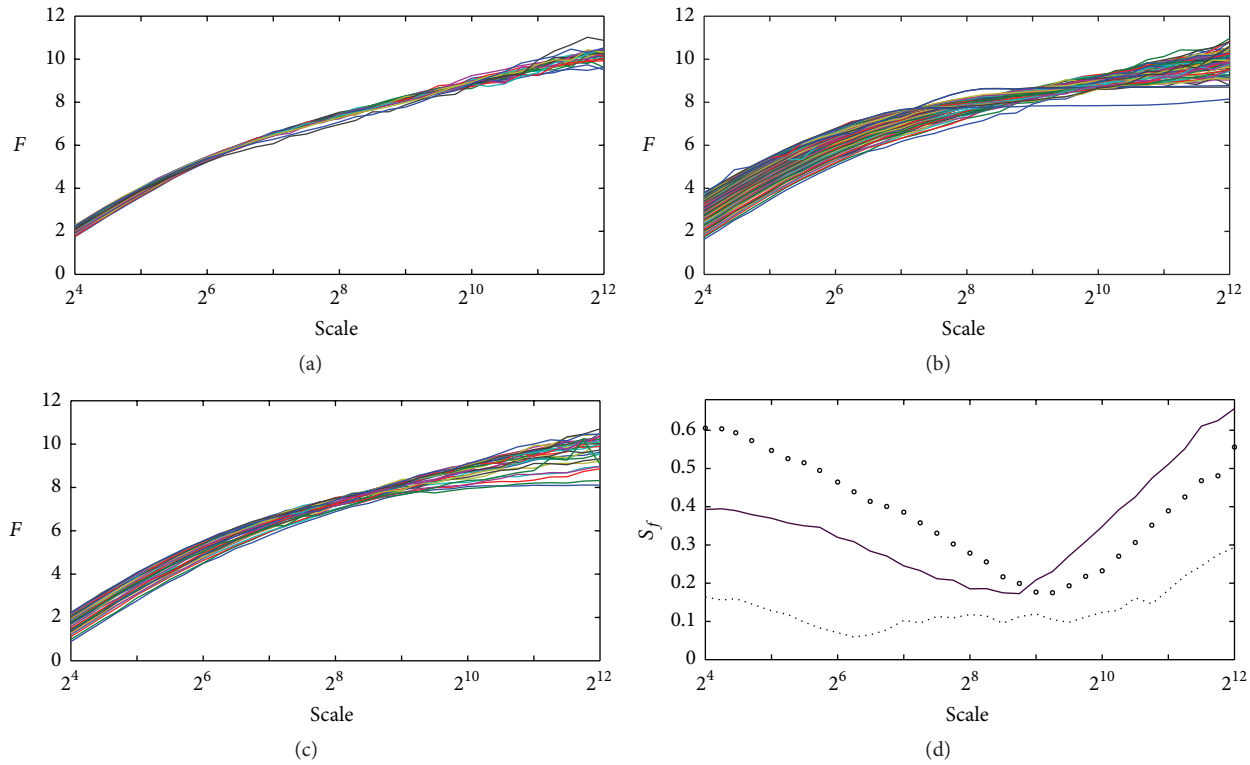

Figure 5: The DFA analysis of the Lorenz time series under different parameters values: (a) σ, (b) ρ, and (c) β and the related standard deviation as a function of the scale in (a) dotted line, (b) circles line, and (c) continuous line.

of displaying a set of curves with respect to the average, the standard deviation is calculated using the following formula:

$$S_f(j) = \sqrt{\frac{1}{m-1}\sum_{i=1}^{m}\left(F^i(j) - \langle F^i(j)\rangle\right)^2}, \qquad (10)$$

where m is the total number of curves in the set (generated by varying the system initial conditions or by varying the system parameter values), $F^i(j)$ is the value of F of the curve i and the scale j, and $\langle F^i(j)\rangle = (1/m)\sum_{i=1}^{m} F^i(j)$ (the average). Figure 4(d) shows that from the scale axis of value 2^5 onward, the standard deviation for F curves from the times series x and y is identical. For not so large scale values, the graphs are near to the average for time series in the case of all the three variables. Approximately, starting from 2^9, the value of $S_f(j)$ begins to grow for the three cases.

To illustrate the response of the DFA algorithm to the parameters of the system presented by (3), the main parameters are varied as follows:

$$6 \le \sigma \le 20 \quad \text{(in steps of 0.5)},$$
$$23 \le \rho \le 100 \quad \text{(in steps of 1.0)},$$
$$0.8 \le \beta \le 3.7 \quad \text{(in steps of 0.1)}.$$

In these parameters' variation, the system stability evolves to one of two equilibrium point attractors with two scrolls. Figure 5 shows the DFA curves for time series when the three parameters are varied. Figures 5(a), 5(b), and 5(c) present the curves for the three variation cases. Figure 5(d) shows the standard deviation of the three cases where it is noticeable that the forms of all curves are similar.

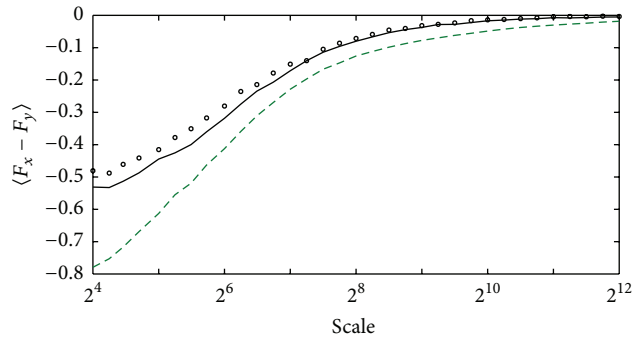

Figure 6: The average of the differences between the DFA of time series $x(t)$ and the DFA of time series $y(t)$ from the Lorenz system at different parameters values: σ is varied (continuous line), ρ is varied (dashed line), and β is varied (circles line).

A comparison of DFA graphs under different parameter values for times series of variable y and time series of variable x is shown in Figure 6. Thus, it contains the average of the difference between detrended fluctuations of time series x and detrended fluctuation of time series y for the three Lorenz main parameters.

The results for the time series of the variable z are presented in Figure 7. It is shown in Figure 7(a) that the

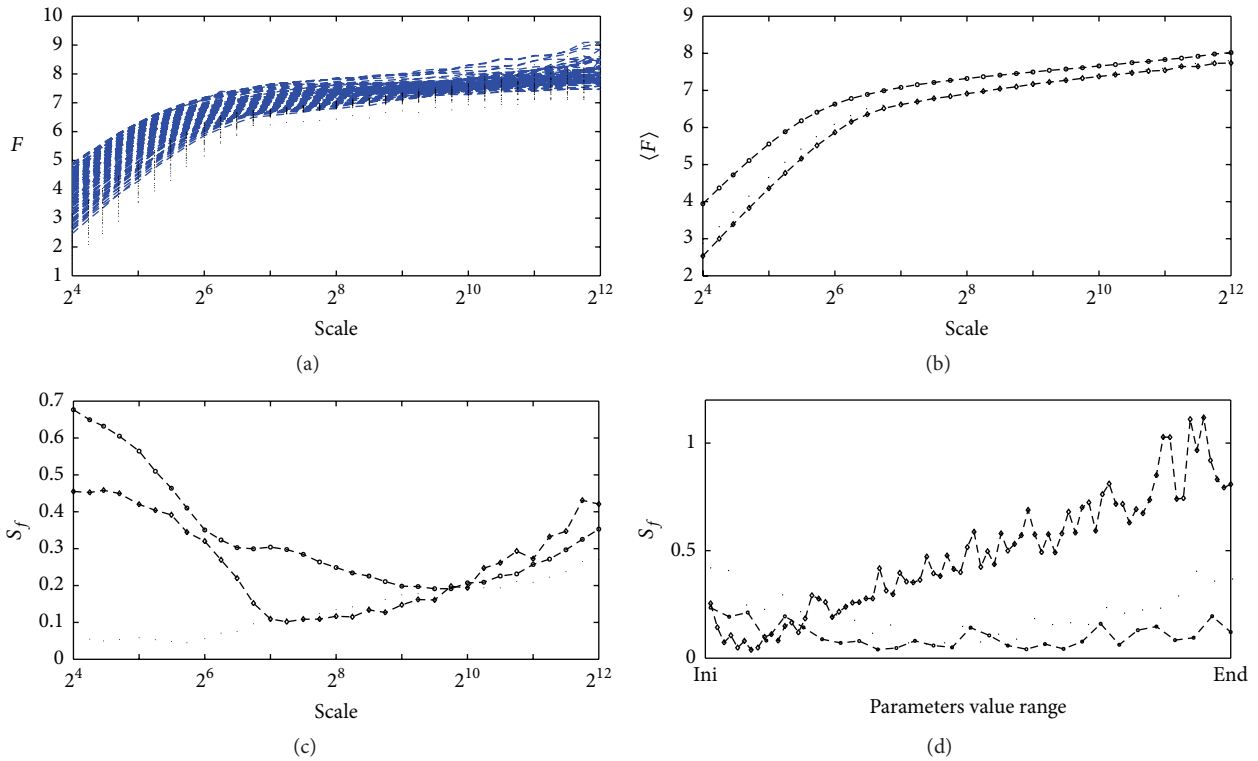

FIGURE 7: The DFA of the variable z (Lorenz system) at different parameter values; in (a) the dashed line and the dotted line correspond to the DFA curves when the parameters ρ and β are varied, respectively; in (b), (c), and (d) the dotted line corresponds to the parameter σ, the dashed line with circles corresponds to the parameter ρ, and the dashed line with diamonds corresponds to the parameter β. The average over the DFA graphs when all Lorenz parameters are varied is presented in (b). The standard deviation as a function of the scale and the parameters value range are presented in (c) and (d), respectively.

DFA curves that correspond to variations of parameter ρ are above the DFA curves that correspond to the parameter β. Furthermore, they have approximately similar shapes with different vertical positions. Thus, when the parameter ρ or β varies, it causes a change in the vertical position of the DFA curve. Figure 7(b) includes the average of each set of the DFA curves determined when the parameter value is varied. The average curves which correspond to every Lorenz parameters begin to be closer when the scale value increases. Meanwhile the standard deviations of the time series fluctuations trend to be the same for the three parameters in large scales (Figure 7(c)), and for larger parameter β values, the standard deviation tends to be bigger than the standard deviation values from the other parameters (Figure 7(d)).

To find the relation between the DFA curves, the correlation coefficient (R) between each pair of DFA curves obtained from time series of an arbitrary variable but at different parameter is defined. The correlation between DFA curves F^i and F^j can be defined as

$$C_{F^iF^j} = \frac{n\sum_{k=1}^{k=n}\left(F^i(k)\,F^j(k)\right) - \left(\sum_{k=1}^{k=n}F^i(k)\right)\left(\sum_{k=1}^{k=n}F^j(k)\right)}{\sqrt{n\sum_{k=1}^{k=n}F^i(k) - \left(\sum_{k=1}^{k=n}F^j(k)\right)^2}\sqrt{n\sum_{k=1}^{k=n}F^j(k) - \left(\sum_{k=1}^{k=n}F^j(k)\right)^2}}, \tag{11}$$

where n is the number of data in the scale. The relationship between ith curve with the rest of other $m-1$ curves generated at different values of a specific parameter is defined as follows:

$$R = \frac{1}{m(m-1)}\sum_{j=1}^{m}\sum_{i=1}^{m}C_{F^iF^j}, \quad \text{for } i \neq j. \tag{12}$$

The correlation coefficient is calculated for DFA curves from time series of the variables x and z. For the variable x the results are 0.9976, 0.9910, and 0.9958 when the parameters σ, ρ, and β are varied, respectively. For the time series z we have 0.9903, 0.9927, and 0.9907 corresponding to the parameters σ, ρ, and β variations, respectively. The presented

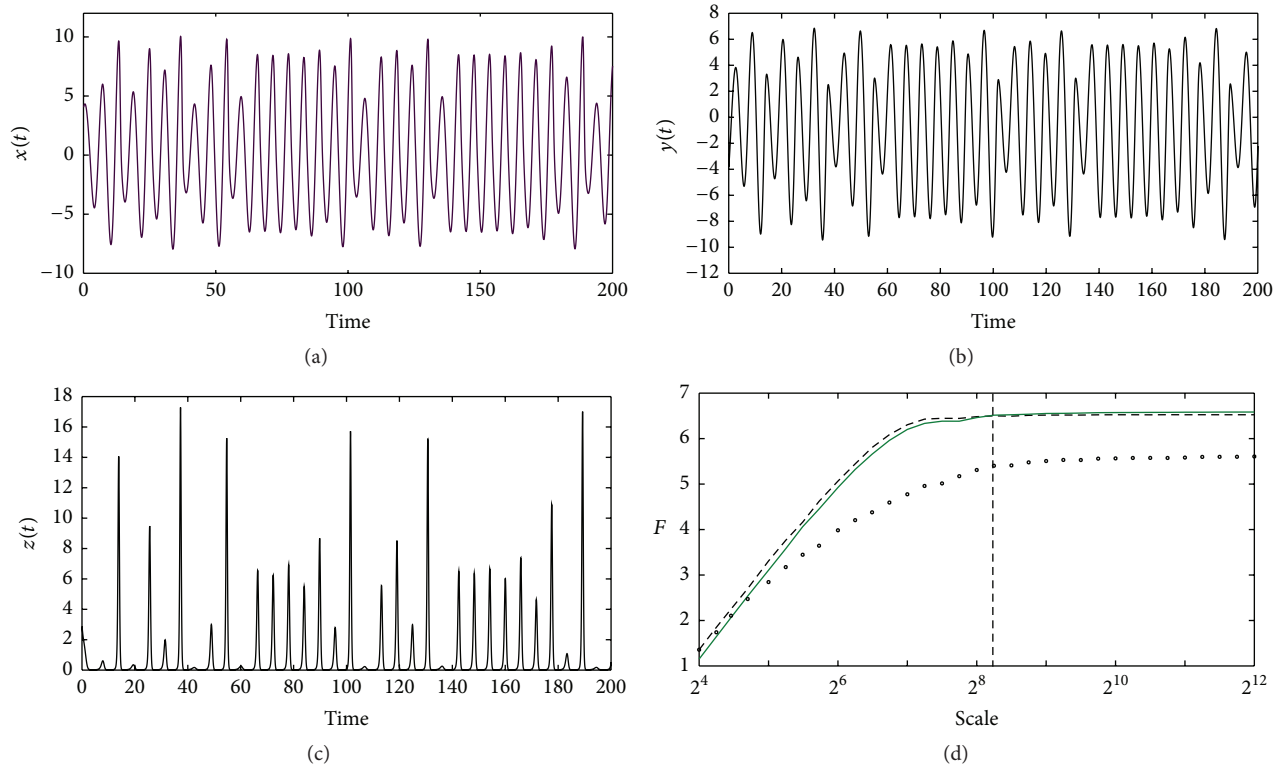

Figure 8: The time series of the Rossler system variables x (a), y (b), and z (c), the DFA of the time series in (d) where the dashed line corresponds to the variable x, the continuous line to variable y, and circles line to the variable z.

numerical results indicate that the DFA algorithm has a constant response and changing the values of the parameter does not affect the stability and the asymptotic behavior of the system.

4.2. Rossler System. The Rossler system can be defined using (8) with the following changes:

$$A = \begin{bmatrix} 0 & -1 & -1 \\ 1 & \rho & 0 \\ 0 & 0 & -\beta \end{bmatrix}, \qquad G(X) = \begin{bmatrix} 0 \\ 0 \\ xz + \gamma \end{bmatrix}, \tag{13}$$

where ρ, β, and γ are the system parameters. Figures 8(a), 8(b), and 8(c) show the Rossler system time series for x, y, and z, respectively, with the parameters values $\rho = 0.2$, $\beta = 5.0$, and $\gamma = 0.2$ at integration step $h = 0.1$.

From the first sight to the DFA algorithm response toward the chaotic time series from Rossler system, it can be seen that the DFA curves of time series x and y are quite similar. On the other hand, the dashed vertical line in Figure 8(d) presents the separation between different behaviors in the time series detected by the DFA algorithm. For scale values smaller than $2^{7.25}$, the values of F slopes are approximately 1.4, 1.5, and 0.92 for the time series x, y, and z, respectively. As a result, at this time scale the DFA algorithm describes the time series x and z as persistent data and the time series from variable y as a Brownian motion. At scale values greater than 2^8 the values of the F slopes are approximately 0.0 for the three time series which leads to conclude that, for large scales, the DFA algorithm characterizes the Rossler time series as a pure antipersistent processes represented by an alternating values sequence.

Figure 9 presents the study of the DFA algorithm response for Rossler time series initialized with the set $-0.8 \leq x(0) \leq 10$ and $-10.0 \leq y(0) \leq 8$ at increments of 1 while z variable initial value is fixed to $z(0) = 3.0$. Figures 9(a), 9(b), and 9(c) contain the set of the DFA graphs under these initial conditions for time series x, y, and z, respectively. As seen in Figure 9, the DFA response for the time series of variable x is similar to the DFA response for time series of variable y. Besides, their respective standard deviations from each set of DFA curves are plotted in Figure 9(d). As expected, the standard deviation of the DFA curves is bigger when the scale value is bigger likewise. In spite of the DFA standard deviation of the curves from the time series z being bigger in comparison with the standard deviation for DFA curves from the time series x and y, the standard deviation of the time series x tends to a small and constant value.

4.3. Multistable System. In the previous subsections, we explore the DFA algorithm response to time series from

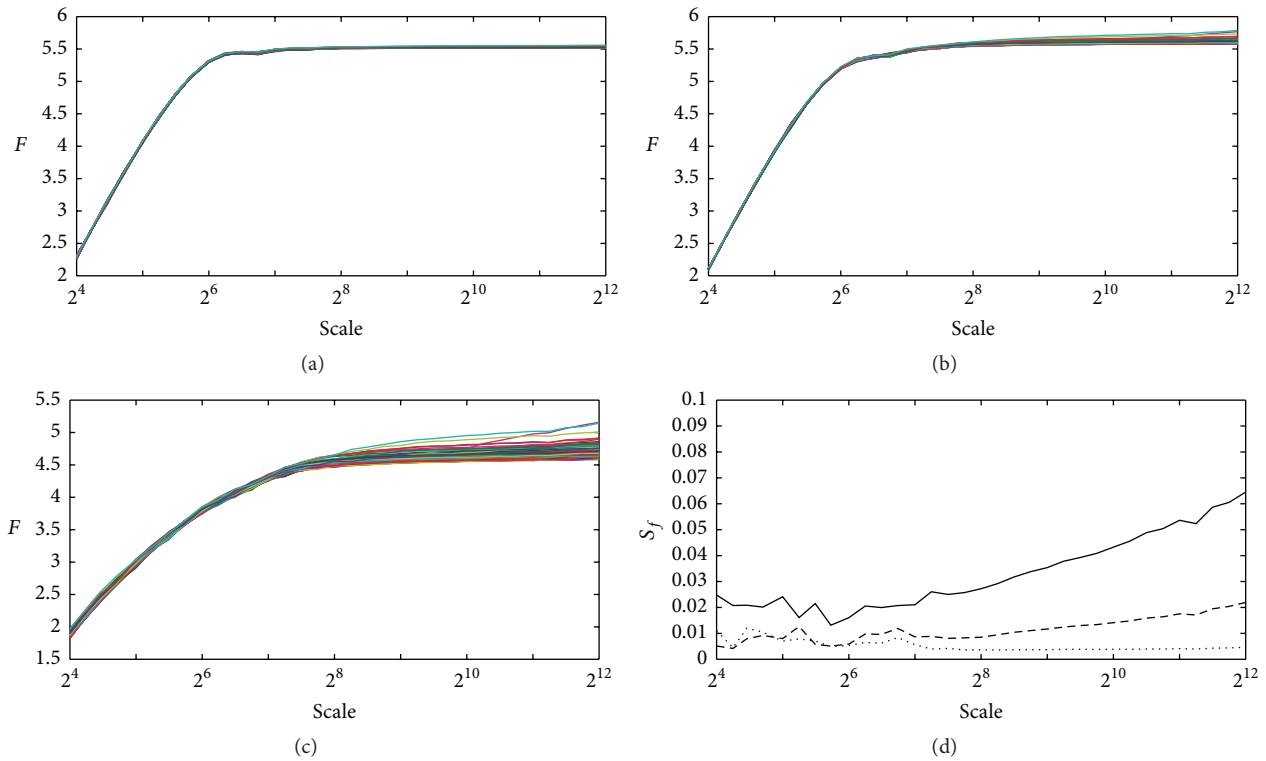

FIGURE 9: The DFA of Rossler system time series under various conditions: (a) time series of the variable x, (b) time series of the variable y, and (c) the time series of the variable z. The standard deviation of each set of curves is presented in (d) where the dotted line corresponds to (a), the dashed line to (b), and continuous line to (c).

chaotic system under the case when $G(\cdot)$ is a nonlinear function. In this section, the time series from a system defined under the case when $G(\cdot)$ is a piecewise linear function; namely, the multistable system is considered. The multistable system is defined as

$$A = \begin{bmatrix} 0 & 1 & 0 \\ 0 & 0 & 1 \\ -\alpha_{31} & \alpha_{32} & -\alpha_{33} \end{bmatrix}, \tag{14}$$

$$G(X) = \begin{bmatrix} 0 \\ 0 \\ u(x) \end{bmatrix}, \tag{15}$$

where α_{31}, α_{32}, and α_{33} are system parameters, and $u : \mathfrak{R} \to \mathfrak{R}$ is the piecewise linear function:

$$u(x) = \begin{cases} 0.9, & \text{if } x \geq 0.3 \\ 0, & \text{if } -0.3 < x < 0.3 \\ -0.9, & \text{if } x \leq -0.3. \end{cases} \tag{16}$$

In [29], it is shown that based on the number of linear pieces in the function $u(x)$, the orbit of the system (14) and (15) could flow with the same number of scrolls.

For the numerical integration made with multistable oscillator, the form (16) is applied and in most cases, the assigned values to the system (14) parameters are chosen to generate orbit solutions with shapes of three scroll oscillators. Figures 10(a), 10(b), and 10(c) present the time series of the multistable oscillator corresponded to the variables x, y, and z generated with a step size $h = 0.1$ and parameter values $\alpha_{31} = 1.5$, $\alpha_{32} = 1.0$, and $\alpha_{33} = 1.0$ ($h = 0.1$ is used in each numerical integration given in this subsection). In Figure 10(d), the DFA corresponding curves are presented where one can see that the persistency of each time series changes as a function of the scale. On the scale interval $[2^4, 2^6)$, the scaling exponents are 1.75, 1.64, and 1.54 for time series x, y, and z, respectively; that is, the DFA algorithm characterizes them as time series with long-range correlation. Meanwhile on the scale interval $(2^7, 2^{12})$, each time series has different characterization. The values of the scaling exponents are 0.8772 (persistent series), 0.2087 (antipersistent), and 0.0144 (antipersistent series oscillating between two values).

Figure 11 shows the results for the DFA response when the initial conditions $(x(0), y(0), z(0))$ of the multistable numerical integration are varied as $-1.0 \leq x(0) \leq 1.0$, $-0.6 \leq y(0) \leq 0.6$, and a constant value for the initial condition $z(0) = 1.0$ with the same parameter values mentioned above. The DFA curves for time series of the three variables are plotted in the same figure (Figure 11). In the interval $[2^4, 2^6]$, the curves are almost overlapped; meanwhile in the interval $[2^6, 2^{12}]$ the set of curves corresponding to time series variable x are located in the upper position, DFA curves for

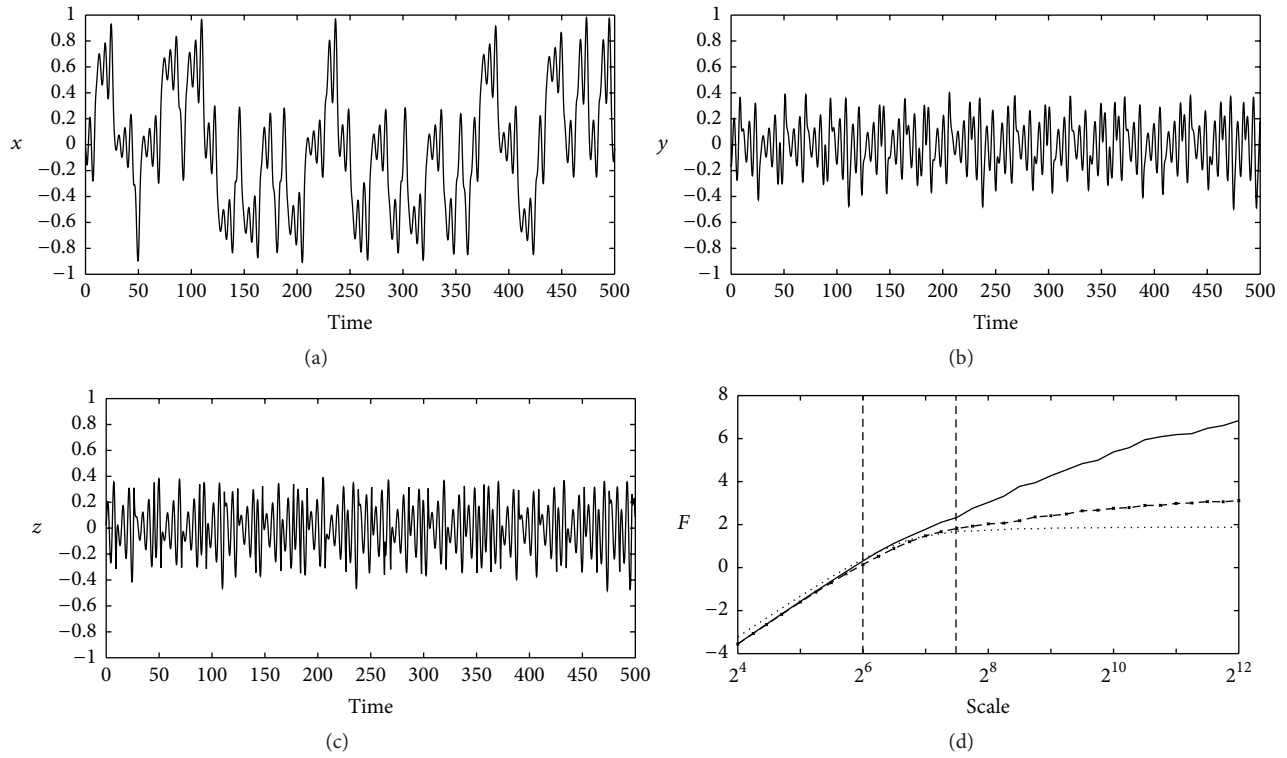

FIGURE 10: The multistable system time series: (a) variable x, (b) variable y, and (c) variable z. (d) shows the DFA for the time series in (a) with continuous line, in (b) with dashed line, and in (c) with dotted line.

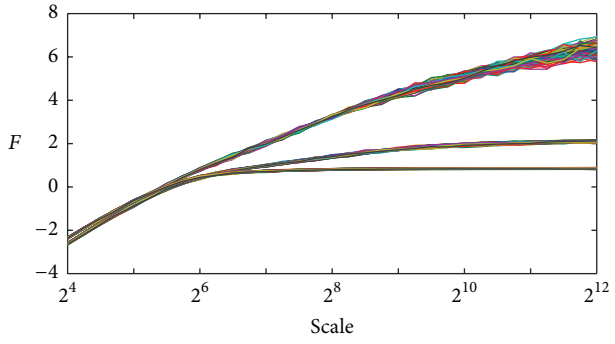

FIGURE 11: The DFA of the time series multistable system generated at various initial conditions.

time series y are in the middle position, and DFA curves for time series z are located in the below position. The error average percentage coefficients $D = (1/m)\sum_{j=1}^{m} S^2(j)$ for each curves set are 2.94%, 0.58%, and 0.37% which correspond to time series of variables x, y, and z, respectively. It is noticeable that these percentages have very small values which indicate that the forms of the curves are similar among them.

Figure 12 shows numerical examples of F graphs from the time series of the three variables of the multistable oscillator when the parameter values are varied and the initial conditions are fixed to (1.5, 1.0, 1.0). The parameter value intervals are selected as a set of values so that the numerically generated orbits with systems (14), (15), and (16) are strange attractors. As in the previous oscillators time series analysis, F graphs from the time series generated under various parameter values have similar form. Figure 12(a) corresponds to the case for F graphs of time series x generated when the parameter α_{31} is varied and the parameters α_{32} and α_{33} are fixed to 1.0. It is easy to see that from the values of scale $> 2^6$, the graphs begin to separate in two groups. Graphs located in the lower positions are generated by varying the parameter α_{31} in the range $1.0 < \alpha_{31} < 1.05$ where the generated orbits with these values are strange attractors with disk form like the one shown in Figure 12(d) (generated with $\alpha_{31} = 1.04$). Graphs located in the above positions are generated with the values $1.05 < \alpha_{31} < 1.53$. Figure 12(b) shows the fluctuation graphs of time series y when the parameter α_{32} value is varied as $1.0 < \alpha_{32} < 1.41$ and the other parameters are fixed to $\alpha_{31} = 1.5$ and $\alpha_{33} = 1.0$. Meanwhile Figure 12(c) shows the fluctuation graphs for time series z generated when the parameter α_{33} varies as $1.0 < \alpha_{33} < 1.47$. Clearly, the DFA curve sets of all figures are adjacent or spliced among them and they change their slope approximately for scale $> 2^7$ values.

Furthermore, to describe the similitude and the closeness among DFA curves, the percent relative standard deviation is used and formulated as

$$S_{\text{rel}} = \frac{\sigma^2\left(F^i(p)\right)}{(1/nm)\sum_{i=1}^{m}\sum_{p=1}^{n} F^i(p)}, \tag{17}$$

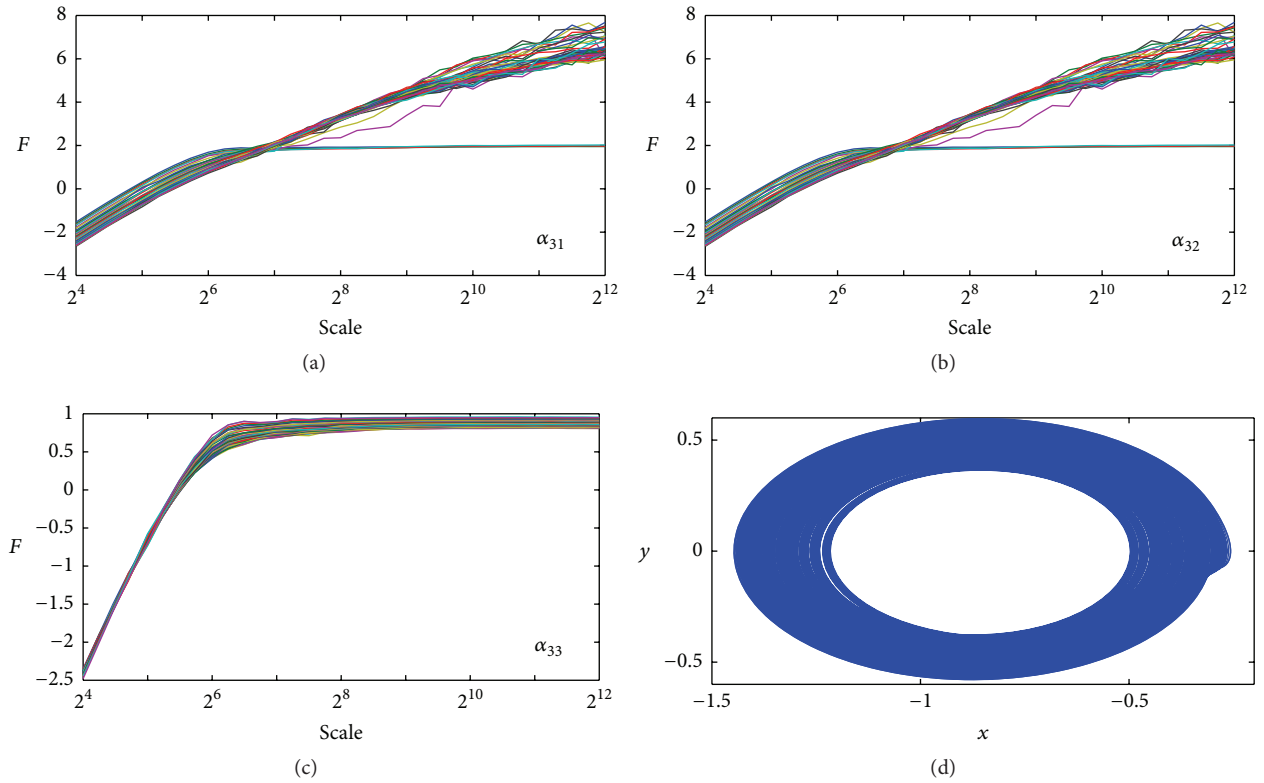

Figure 12: The DFA of the time series multistable system generated at different parameters values: (a) variable α_{31}, (b) variable α_{32}, and (c) variable α_{33}. (d) presents the multistable strange attractor which revolves around one fixed point.

Table 1: Relative standard deviation of the DFA curves calculated with different parameter values.

Parameter	Variable	S_{rel} (%)
α_{31}	x	0.103
	y	0.066
	z	0.022
α_{32}	x	2.31
	y	4.14
	z	7.04
α_{33}	x	3.76
	y	1.72
	z	0.64

where m is the number of different values assigned to a specific parameter, n is the number of scales, and σ^2 is the variance. In Table 1, the relative standard deviations of each set of DFA curves are presented where a set of curves is obtained by analyzing the time series of the same variable at different parameter values. As we can see in the right column of Table 1 (S_{rel} (%)), the DFA curves are not dispersed.

A more complete analysis for the time series of the system defined by (14), (15), and (16) is listed in Table 2 where the average of scaling exponents and the relative standard deviations as a function of the parameter value interval (second column) and the scale interval (third column) are presented. As we can see, the parameter α_{31} has only two parameter intervals. The interval $[1.0, 1.04)$ corresponds to multistable oscillator graphs with only one scroll like the plot in Figure 12(d). Meanwhile, the interval $[1.05, 1.53]$ corresponds to triple scroll oscillators. As a consequence, the scaling exponents are different from each other. Besides, Table 2 shows that from the small scale ($[2^4, 2^6]$) to the large scale ($[2^7, 2^{12}]$), each time series decreases its scaling exponent value. With respect to the parameter α_{31} in the interval $[1.0, 1.04]$, the scaling exponent average of the sets of time series for variables x and y becomes zero at large scales because their time series are oscillating signals with amplitude that varies very slowly. For time series y, the DFA algorithm characterizes the change from series with long-range correlation (small scales) to antipersistent series (large scales). For time series z from triple scroll oscillator, the DFA algorithm characterizes the change from persistent series (small scales) to series oscillating between two values (large scale). Finally, for the cases with $S_{rel} > 20\%$, this value does not mean that the DFA curve slopes are greatly expanded over the average. The real reason behind this case is that the scaling exponent averages are very close to zero ($\overline{\alpha} \to 0$).

Table 2: The scaling exponent average of the DFA curves and their respective relative standard deviation for multistable system time series generated with various parameter values. The behavior column abbreviations: P: persistent; AP: antipersistent; AP2: antipersistent oscillating between two values; LRC: long range correlation. The symbol "+" in the case of LRC and P refers to the set of the DFA curves contain time series that behaves as Brownian motion.

Parameter	Interval value	Scale	Variable	$\overline{\alpha}$	S_{rel} (%)	Behavior
α_{31}	(1.0, 1.04)	$[2^4, 2^6]$	x	1.64	0.25	LRC
			y	1.64	0.20	LRC
			z	1.63	0.33	LRC
		$[2^7, 2^{12}]$	x	0.03	49.41	AP2
			y	0.00	4.7	AP2
			z	0.00	11.42	AP2
	[1.05, 1.53]	$[2^4, 2^6]$	x	1.69	1.20	LRC
			y	1.58	1.37	LRC
			z	1.49	3.23	P+
		$(2^7, 2^{12})$	x	0.91	11.50	P
			y	0.21	12.88	AP
			z	0.01	25.57	AP2
α_{32}	(1.0, 1.40]	$[2^4, 2^6]$	x	1.63	3.26	LRC
			y	1.51	1.76	LRC+
			z	1.43	0.80	P
		$[2^7, 2^{12}]$	x	0.90	9.20	P
			y	0.22	8.05	AP
			z	0.01	29.5	AP2
α_{33}	[1.0, 1.47]	$[2^4, 2^6]$	x	1.70	1.20	LRC
			y	1.58	1.43	LRC
			z	1.49	3.39	P+
		$[2^7, 2^{12}]$	x	0.89	10.94	AP
			y	0.21	11.33	AP
			z	0.01	24.00	AP2

5. DFA Algorithm for Fine Spectrum Sensing

As mentioned before, the DFA algorithm is used for fine SS (PU signal detection) in two-stage spectrum sensor. This idea is proposed based on the DFA algorithm behavior analysis presented in Sections 3 and 4. The DFA algorithm performance and response are stable and invariant under different initial conditions and for different chaotic system parameters. The last important property (DFA response robustness against the changes of the initial conditions and parameters) made the use and implementation of the DFA algorithm for fine SS a very practical solution under various types of imperfections that change the initial conditions of the SS process such as spatial correlation between the antenna array elements and noise variance uncertainty. Additionally, one of the main conclusions from the presented analysis in Sections 3 and 4 that the DFA algorithm stability, reliability, and immunity toward the fluctuations in the initial conditions is maintained at the expense of relatively large number of samples. As a result, the DFA is implemented for fine SS and not for coarse SS. A brief summary about the last discussion can be found in Figure 13.

These two sensing stages can be performed in serial or parallel modes. For serial mode, if the ED decides that there is PU signal in a certain radio channel, the fine sensing stage is eliminated or aborted. Otherwise, the fine sensing stage is performed on the same radio channel for the final decision. In the case of parallel mode, the two sensing stages are performed in parallel and the final decision about the PU signal presence or absence is made by combining the decisions of the two stages. The block diagram of the proposed spectrum sensor is shown in Figure 14 where the ED is implemented for the coarse or fast SS and the fine SS is performed by the DFA.

5.1. System Model. In the bandwidth of the spectrum to be sensed there are number of radio channels equal to N_{ch} and all these channels are serially sensed. The proposed spectrum sensor is equipped by antenna array with the number of elements equal to M and each antenna array element receives N samples during the sensing time. The ED accumulates the energy of MN samples and compares it to the ED threshold (THR_{ED}) to decide the PU signal presence or absence. The times required for coarse sensing t_{s1} and for fine sensing t_{s2} per each channel are given by

$$t_{s1} = \frac{N_{s1}}{2W}, \qquad t_{s2} = \frac{N_{s2}}{2W}, \tag{18}$$

where N_{s1} and N_{s2} are the numbers of samples needed for coarse and fine sensing, respectively, and W is the channel bandwidth. Since $N_{s2} > N_{s1}$ then it is axiomatic that $t_{s2} > t_{s1}$. In the case if the two sensing stages are performed in parallel mode, the total sensing time for all radio channels is defined as

$$T_{\text{total}} = N_{\text{ch}} \frac{N_{s1}}{2W} + \overline{N_{\text{fs}}} \frac{N_{s2}}{2W}, \tag{19}$$

where N_{ch} is the total number of radio channels to be sensed and $\overline{N_{\text{fs}}}$ is the mean number of the reported radio channels for the fine sensing stage. The PU signal detection problem (spectrum sensing) can be presented using the conventional binary hypothesis test:

$$\begin{aligned} H_0 &\Longrightarrow x_i[k] = n_i[k], \\ &\qquad i = 1, \ldots, M;\ k = 0, \ldots, N-1, \\ H_1 &\Longrightarrow x_i[k] = h_i[k]\, s_i[k] + n_i[k], \\ &\qquad i = 1, \ldots, M;\ k = 0, \ldots, N-1, \end{aligned} \tag{20}$$

where $x_i[k]$ is the discrete-time received signal at the input; $n_i[k]$ is the discrete-time colored noise (filtered noise samples) with zero mean and variance σ_n^2, that is, $n_i[k] \sim \mathcal{CN}(0, \sigma_n^2)$; $h_i[k]$ is the discrete-time channel coefficients

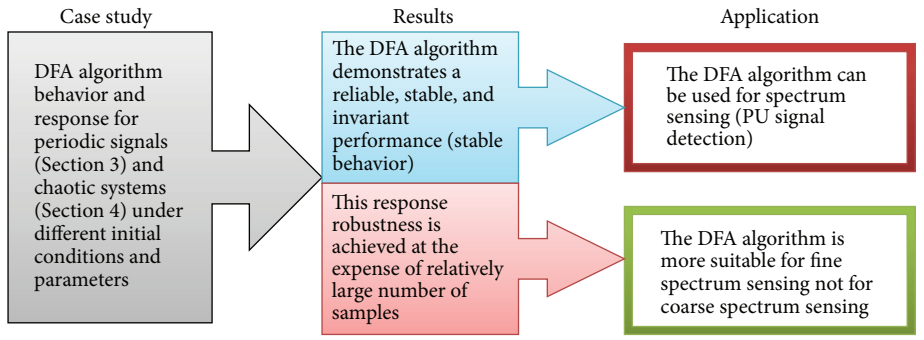

Figure 13: A brief summary about the DFA algorithm studying results and the related application.

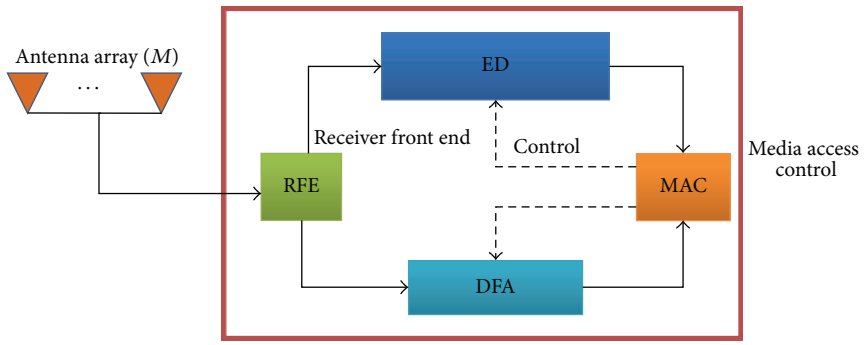

Figure 14: Two-stage spectrum sensing using ED and DFA.

obeying the circularly symmetric complex Gaussian distribution with zero mean and variance equal to σ_h^2, that is, $h_i[k] \sim \mathcal{CN}(0, \sigma_h^2)$; and $s_i[k]$ is the discrete-time PU signal. The channel coefficients $h_i[k]$ are spatially correlated between each other. The coefficient of spatial correlation C_{sc} between the adjacent antenna array elements ($0 \leq C_{sc} \leq 1$) can be given as [30]

$$C_{sc} = \exp\left[-23\Lambda^2\left(\frac{d}{\lambda}\right)^2\right], \tag{21}$$

where λ is the wavelength; d is the distance between two adjacent antennas; and Λ is defined as

$$\Lambda = \frac{\sqrt{\theta^2 + 2\cos(\theta) - 2}}{2\theta}, \tag{22}$$

where θ is the angular spread. The components of the $M \times M$ antenna array element correlation matrix $\mathbf{C}$ can be presented in the following form:

$$\mathbf{C}_{ij} = \left\{C_{sc}^{\,i-j}\right\}, \quad i \leq j,\ i, j = 1, \ldots, M. \tag{23}$$

The $NM \times 1$ signal vector $\mathbf{X}$ that collects all the observed signal samples during the sensing time can be defined using the following form:

$$\mathbf{X} = [\mathbf{x}_1[0], \ldots, \mathbf{x}_M[0], \ldots, \mathbf{x}_1[N-1], \ldots, \mathbf{x}_M[N-1]]^T, \tag{24}$$

where T denotes a transpose. The data distribution of the matrix $\mathbf{X}$ can be expressed as

$$\mathbf{X} \sim \begin{cases} \mathcal{CN}\left(0, \sigma_n^2\mathbf{I}\right) \Longrightarrow H_0; \\ \mathcal{CN}\left(0, E_s\sigma_h^2\mathbf{I} + \sigma_n^2\mathbf{I}\right) \Longrightarrow H_1, \end{cases} \tag{25}$$

where E_s is the average energy of the PU signal and $\mathbf{I}$ is the $MN \times MN$ identity matrix.

5.2. Fine Spectrum Sensing Using DFA. In general, the radio channel with low power has a high probability to be unused by the PU. The fine sensing stage in this scheme is performed owing to the fact that the ED threshold definition is susceptible to noise power variations and as a consequence, its detection performance. The DFA algorithm behaves differently if the input data, in this case $\mathbf{X}$, contains noise samples only (the hypothesis H_0) or contains samples of PU signal plus noise (the hypothesis H_1). The test statistics based on the DFA algorithm is highly attached to the output parameter or the scaling exponent α given by (6). Thus, the DFA test statistics $T_{DFA}(\mathbf{X})$ can be defined using the following form:

$$T_{DFA}(\mathbf{X}) = \begin{cases} \alpha = 0.5 \Longrightarrow H_0 \\ \alpha \neq 0.5 \Longrightarrow H_1. \end{cases} \tag{26}$$

Under the hypothesis H_0, the value of the scaling exponent α of the DFA algorithm indicates that the input data corresponds to random or stochastic process like colored noise

Table 3: The final decision making rule of two stages SS using "OR" rule.

ED	DFA	Final
H_0	H_1	H_1
H_1	H_0	H_1
H_1	H_1	H_1
H_0	H_0	H_0

samples. Under the alternative hypothesis (H_1), the scaling exponent α value indicates that input data corresponds to correlated data samples (not only noise) which leads us to conclude that it contains samples of signal plus noise. These results are obtained since the modulated signals have cyclostationary features when the mean and the autocorrelation function exhibit periodicity.

The final decision about the PU signal presence or absence is obtained by combining the decisions of the two stages using the decision making rule. For example, if the "OR" rule is used, Table 3 presents the two sensing stages final decision making results.

In the case of two-stage spectrum sensing scheme, the probability of false alarm P_{FA} and the probability of detection P_D are defined with the respect to the two stages test statistics. Under the hypothesis H_0, if $T_{\text{ED}}(\mathbf{X}) > \text{THR}_{\text{ED}}$ or if $\alpha \neq 0.5$ when $T_{\text{ED}}(\mathbf{X}) \leq \text{THR}_{\text{ED}}$, the false alarm occurs, where $T_{\text{ED}}(\mathbf{X})$ is the ED test statistics given by

$$T_{\text{ED}}(\mathbf{X}) = \sum_{k=0}^{N-1} \sum_{i=1}^{M} x_i^2 [k] \underset{H_0}{\overset{H_1}{\gtrless}} \text{THR}_{\text{ED}}. \tag{27}$$

The correct PU detection occurs under the hypothesis H_1, if $T_{\text{ED}}(\mathbf{X}) > \text{THR}_{\text{ED}}$ or if $\alpha \neq 0.5$ given that $T_{\text{ED}} \leq \text{THR}_{\text{ED}}$. Thus, the overall value can be defined as

$$\begin{aligned} P_{\text{FA}} &= P_{\text{FA}}^{\text{ED}} + \left(1 - P_{\text{FA}}^{\text{ED}}\right) P_{\text{FA}}^{\text{DFA}}, \\ P_D &= P_D^{\text{ED}} + \left(1 - P_D^{\text{ED}}\right) P_D^{\text{DFA}}, \end{aligned} \tag{28}$$

where $P_{\text{FA}}^{\text{ED}}$ and P_D^{ED} are the probability of false alarm and the probability of detection of the first sensing stage using ED, respectively, and $P_{\text{FA}}^{\text{DFA}}$ and P_D^{DFA} are the probabilities of false alarm and detection of the second stage using DFA, respectively.

5.3. Fine Spectrum under Noise Power Uncertainty. The second type of imperfections after the spatial correlation between the adjacent antenna array elements is the noise power or variance uncertainty. The sensitivity to noise power uncertainty (the fluctuations on the noise variance value as a function of time) is one of the most common problems among the spectrum sensors such as the energy detector (ED), matched filter (MF), and even the cyclostationary detector under the low signal-to-noise ratio (SNR) [31, 32]. The negative effect of noise power uncertainty is quantified by the SNR wall location. If the SNR value is less than the SNR wall, the PU signal detector (spectrum sensor) will fail to achieve the desired detection performance and maintain the immunity against power noise uncertainty regardless of the sensing time length. This problem negatively affects the receiver operation characteristic (ROC).

The SNR wall phenomenon can be presented using the sampling complexity of the spectrum sensor that is defined as the number of samples N as a function of the SNR, the probability of false alarm P_{FA}, and probability of miss P_{miss}:

$$N = f\left(\text{SNR}, P_{\text{FA}}, P_{\text{miss}}\right). \tag{29}$$

In general, any spectrum sensor (or the PU signal detector) must minimize the number of samples N required to achieve the desired detection performance. The lowest SNR satisfying the probability of false alarm P_{FA} and the probability of miss P_{miss} constraints is called the detector sensitivity.

Under noise power uncertainty initial conditions, the actual noise power or variance σ^2 at the spectrum sensor input can be determined only within the limits of a definite range [31]:

$$\sigma^2 \in \left[\frac{1}{\rho}\sigma_n^2, \rho\sigma_n^2\right], \tag{30}$$

where ρ is the uncertainty parameter defined as

$$\rho = 10^{0.1\varepsilon}, \tag{31}$$

where ε is the parameter used to define the amount of nonprobabilistic uncertainty in the noise power. Clearly, small values of ε (least uncertainty case) are preferred. As an example, the sampling complexity of the ED can be defined using the uncertainty parameter ρ as follows:

$$N_{\text{ED}} = \frac{\left[\rho Q^{-1}\left(P_{\text{FA}}^{\text{ED}}\right) - \rho^{-1} Q^{-1}\left(1 - P_{\text{miss}}^{\text{ED}}\right)\right]^2}{M\left[\text{SNR} - \left(\rho - \rho^{-1}\right)\right]^2}, \tag{32}$$

where

$$Q(x) = \frac{1}{\sqrt{2\pi}} \int_x^{\infty} \exp\left(-\frac{1}{2}t^2\right) dt \tag{33}$$

is the Gaussian Q-function. From (32), we can define the ED SNR wall in the following form [31]:

$$\text{SNR}_{\text{wall}}^{\text{ED}} = \frac{\rho^2 - 1}{\rho}. \tag{34}$$

With the new initial conditions when there is noise power uncertainty, the data distribution of the matrix $\mathbf{X}$ given by (25) should be modified to consider the uncertainty parameter ρ (the actual noise power σ^2):

$$\mathbf{X} \sim \begin{cases} \mathcal{CN}\left(0, \sigma^2\mathbf{I}\right), & \sigma^2 \in \left[\frac{1}{\rho}\sigma_n^2, \rho\sigma_n^2\right] \Longrightarrow H_0; \\ \mathcal{CN}\left(0, E_s\sigma_h^2\mathbf{I} + \sigma^2\mathbf{I}\right), & \sigma^2 \in \left[\frac{1}{\rho}\sigma_n^2, \rho\sigma_n^2\right] \Longrightarrow H_1. \end{cases} \tag{35}$$

As a result, the sample complexity tends to approach infinity as the SNR decreases to approach the SNR wall:

$$\lim_{\text{SNR} \to \text{SNR}_{\text{wall}}} f\left(\text{SNR}, P_{\text{FA}}, P_{\text{miss}}, \rho\right) \longrightarrow \infty. \tag{36}$$

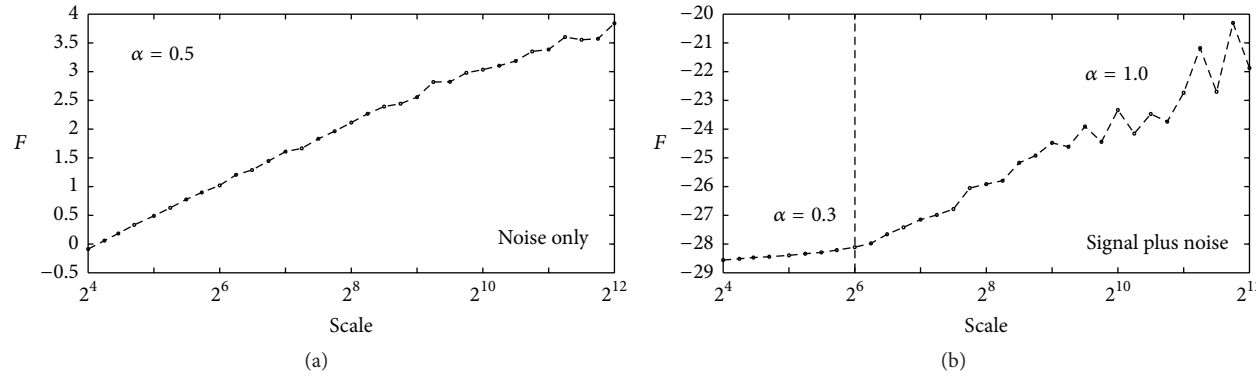

Figure 15: The DFA algorithm behavior under two cases: (a) the data matrix **X** contains samples from noise only; (b) the data matrix **X** contains samples from signal plus noise under spatial correlation between antenna array elements.

Table 4: The main simulation parameters.

Parameter	Value
Number of antenna array elements	$M = 6$
Signal-to-noise ratio	SNR = −10 [dB]
The angular spread	$\theta = 0.5^{\circ}$
Distance between adjacent antenna elements	$d = \lambda/8$
Coefficient of spatial correlation	$C_{sc} = 1$
Nonprobabilistic uncertainty parameter	$\varepsilon = 1$ [dB]
Channel parameter	$\sigma_h^2 = 1$
The scale (number of samples N)	Variable

It is important to mention that the SNR at the input of the spectrum sensor is defined using the following form:

$$\text{SNR} = \frac{E_s \sigma_h^2}{\sigma^2}. \tag{37}$$

As seen from (30) and (37), the noise power uncertainty leads to SNR value uncertainty at the spectrum sensor input.

5.4. Numerical Results. The main objective of this section is to show how the DFA algorithm behaves differently in accordance with the input data, in this case the data matrix **X** of the observed received signal samples at the spectrum sensor input. In other words, the DFA response and the value of the scaling exponent (test statistics) differ with a considerable way when **X** contains data samples from noise only or data samples from PU signal plus noise (see Figure 15). This fact about the DFA algorithm behavior is illustrated in Figure 15 where in Figure 15(a) the data matrix (DFA input) is formed from noise samples only and in Figure 15(b) the data matrix is formed from PU signal plus noise samples. The simulation results are obtained using the parameters given in Table 4. Note that in this section, the value of scale is equal to the number of samples N. The DFA performance as a fine spectrum sensor is shown by following the same evaluation approach presented in Sections 3 and 4.

As shown in Figure 15, the DFA algorithm responses and behaves differently in accordance with the input data matrix **X** contents in the presented two cases, namely, noise only (a) and PU signal plus noise (b). As a direct observation about the test statistics presented in (26), the value of the scaling exponent α in the case of noise is 0.5 ((a), $\alpha = 0.5$) while in the case of noise plus signal this value is not equal to 0.5 ((b), $\alpha \neq 0.5$). It is important to mention that the value of the scaling exponent α changes in Figure 15(b) according to the scale range. For instance, when the Scale $\leq 2^6$ the scaling exponent $\alpha = 0.3$ and when the Scale $> 2^6$ the scaling exponent $\alpha = 1.0$.

Under two types of imperfections, namely, spatially correlated antenna array elements and noise power uncertainty, the DFA response is illustrated in Figure 16 when the value of the ε is equal to 1 dB (this parameter value is chosen to roughly give a big noise power uncertainly when in the case of ED we have that $\text{SNR}_{\text{wall}}^{\text{ED}} = -3$ dB).

From Figure 16, it is confirmed that the DFA algorithm performance differs according to the input data type of the matrix **X**. For instance, in the case of noise only as shown in Figure 16(a), the value of the scaling exponent α is equal to 0.5 ($\alpha = 0.5$) even under uncertainty case. The attention should be paid to the case of PU signal plus noise presented in Figure 16(b) at two types of imperfections, namely, spatially correlated antenna array elements and noise power uncertainty when the scaling exponent has two values ($\alpha \neq 0.5$) according to the number of samples (the scale range). Approximately, when the Scale $\leq 2^9$ the scaling exponent $\alpha = 0.24$ and when the Scale $> 2^9$ the scaling exponent $\alpha = 2.0$. Thus, the DFA algorithm is still able to distinguish between the basic binary hypothesis cases (H_0 and H_1) even under the combined extreme conditions of spatial correlation and noise uncertainty. Comparing the last two cases presented in Figure 15 (spatial correlation case) and Figure 16 (combined spatial correlation and noise uncertainty case), it is clear that the scale and the scaling exponent have different limits and values.

A complete analysis for the DFA employment in fine spectrum sensing (full theoretical analysis with detailed performance comparison with other spectrum sensing algorithms) requires a special dedicated work that can be considered as a future work for the authors.

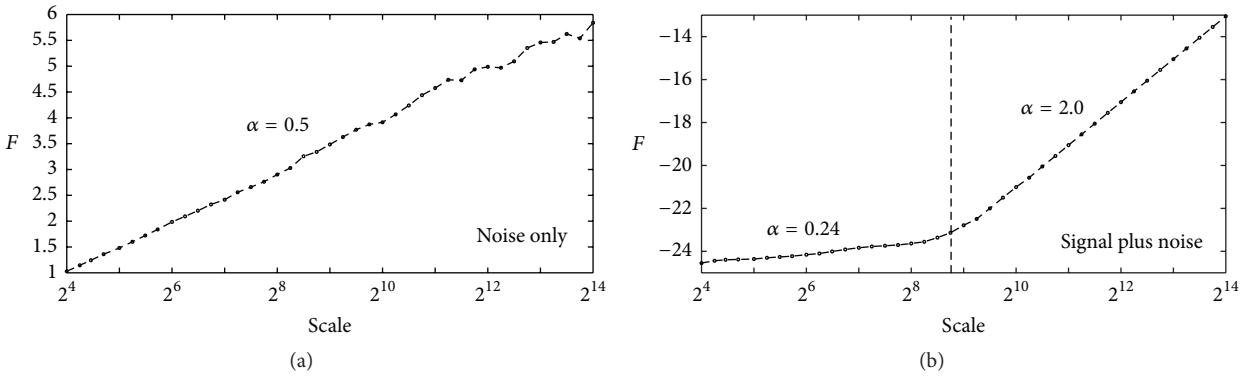

Figure 16: The DFA algorithm behavior under two cases: (a) the data matrix **X** contains samples from noise only; (b) the data matrix **X** contains samples from signal plus noise under two types of imperfections (spatial correlation and noise uncertainty).

6. Conclusions

In this work, a numerical study about the DFA algorithm response and behavior toward the periodical and chaotic signals is discussed. According to the presented results, each signal can have more than one characterization that depends on the time scale under analysis. For example, in the case of short signal intervals (small scales), the DFA algorithm characterizes the signals as periodic or persistent. For periodical signals like sinusoidal, the slope of the detrended fluctuation graphs changes its value to zero when the scale reaches the first period of the signal. For chaotic signals (not periodic), the DFA characterizes them as periodic at small time scales.

The presented results have evidently demonstrated that the DFA response is invariant and robust to initial condition and chaotic system parameters. For several numerical proofs, the results were very similar when the initial conditions of the orbit are varied and the system parameters are changed. As a result, it is possible to characterize the persistency (or antipersistency) of time series from real systems (like physical systems, social system, biological, etc.) without the need of performing and repeating large number of experiments.

A primitive proposal about using the DFA algorithm for fine spectrum sensing along with ED (coarse stage) in two-stage topology is presented. The DFA does not require any prior knowledge of the PU signal parameters and relies only on the data matrix of the sampled received signal. The test statistics of the DFA fine spectrum sensing is simple and based on the main algorithm output, namely, the scaling exponent. The numerical outcomes show promising results about futuristic use of DFA algorithm for spectrum sensing in CR systems under practical imperfections like noise power uncertainty and spatially correlated antenna array elements.

Competing Interests

The authors declare that there are no competing interests regarding the publication of this paper and also regarding the funding that they have received.

Acknowledgments

This research is supported by the National Council of Science and Technology in Mexico (Consejo Nacional de Ciencia y Tecnología CONACYT) with research Grant no. 35022. Additionally, this work is performed by Radio Physics Research Group (RPRG) at Polytechnic University of San Luis Potosi (UPSLP), San Luis Potosi, Mexico.

References

[1] P. Talkner and R. O. Weber, "Power spectrum and detrended fluctuation analysis: application to daily temperatures," *Physical Review E*, vol. 62, no. 1, pp. 150–160, 2000.

[2] M. V. Sewell, "The efficient market hypothesis: empirical evidence," *International Journal of Statistics and Probability*, vol. 1, no. 2, pp. 164–178, 2012.

[3] R. Chiaruccia, F. Ruzzenentia, and M. I. Loffredoa, "Detecting spatial homogeneity in the World Trade Web with Detrended Fluctuation Analysis," *Physica A*, vol. 401, pp. 1–7, 2014.

[4] P. M. Ashton, G. A. Taylor, M. R. Irving, I. Pisica, A. M. Carter, and M. E. Bradley, "Novel application of detrended fluctuation analysis for state estimation using synchrophasor measurements," *IEEE Transactions on Power Systems*, vol. 28, no. 2, pp. 1930–1938, 2013.

[5] R. A. Ribeiro, M. V. M. Mata, L. S. Lucena, U. L. Fulco, and G. Corso, "Spatial analysis of oil reservoirs using detrended fluctuation analysis of geophysical data," *Nonlinear Processes in Geophysics*, vol. 21, no. 5, pp. 1043–1049, 2014.

[6] S. M. Lachowycz, D. M. Pyle, T. A. Mather et al., "Long-range correlations identified in time-series of volcano seismicity during dome-forming eruptions using detrended fluctuation analysis," *Journal of Volcanology and Geothermal Research*, vol. 264, pp. 197–209, 2013.

[7] F. Febriani, P. Han, C. Yoshino et al., "Ultra low frequency (ULF) electromagnetic anomalies associated with large earthquakes in Java Island, Indonesia by using wavelet transform and detrended fluctuation analysis," *Natural Hazards and Earth System Science*, vol. 14, no. 4, pp. 789–798, 2014.

[8] H. G. Schuster, *Deterministic Chaos: An Introduction*, VCH, Weinheim, Germany, 1988.

[9] H. D. I. Abarbanel, *Analysis of Observed Chaotic Data*, Springer, 1995.

[10] J. Alvarez-Ramirez, E. Rodriguez, J. C. Echeverria, and H. Puebla, "Correlation analysis of chaotic trajectories from Chua's system," *Chaos, Solitons and Fractals*, vol. 36, no. 5, pp. 1157–1169, 2008.

[11] Z. Chen, P. C. Ivanov, K. Hu, and H. E. Stanley, "Effect of nonstationarities on detrended fluctuation analysis," *Physical Review E*, vol. 65, no. 4, Article ID 041107, pp. 1–15, 2002.

[12] Z. Chen, K. Hu, P. Carpena, P. Bernaola-Galvan, H. E. Stanley, and P. C. Ivanov, "Effect of nonlinear filters on detrended fluctuation analysis," *Physical Review E*, vol. 71, no. 1, Article ID 011104, 11 pages, 2005.

[13] C. Heneghan and G. McDarby, "Establishing the relation between detrended fluctuation analysis and power spectral density analysis for stochastic processes," *Physical Review E: Statistical Physics, Plasmas, Fluids, and Related Interdisciplinary Topics*, vol. 62, no. 5, pp. 6103–6110, 2000.

[14] R. U. Acharya, C. M. Lim, and P. Joseph, "Heart rate variability analysis using correlation dimension and detrended fluctuation analysis," *ITBM-RBM*, vol. 23, no. 6, pp. 333–339, 2002.

[15] P. Oświęcimka, J. Kwapień, and S. Drożdż, "Wavelet versus detrended fluctuation analysis of multifractal structures," *Physical Review E*, vol. 74, no. 1, Article ID 016103, 37 pages, 2006.

[16] M. Sozanski and J. Zebrowki, "On the application of DFA to the analysis of unimodal maps," *Acta Physica Polonica B*, vol. 36, no. 5, pp. 1803–1822, 2005.

[17] W. P. He, G. L. Feng, Q. Wu, S. Q. Wan, and J. F. Chou, "A new method for abrupt change detection in dynamic structures," *Nonlinear Processes in Geophysics*, vol. 15, no. 4, pp. 601–606, 2008.

[18] Y. Liu, G. Yang, M. Li, and H. Yin, "Variational mode decomposition denoising combined the detrended fluctuation analysis," *Signal Processing*, vol. 125, pp. 349–364, 2016.

[19] A. Mert and A. Akan, "Detrended fluctuation thresholding for empirical mode decomposition based denoising," *Digital Signal Processing: A Review Journal*, vol. 32, pp. 48–56, 2014.

[20] S. Miriyala, P. R. Koppireddi, and S. R. Chanamallu, "Robust detection of ionospheric scintillations using MF-DFA technique," *Earth, Planets and Space*, vol. 67, article 98, 2015.

[21] S. K. Sharma, T. E. Bogale, S. Chatzinotas, B. Ottersten, L. B. Le, and X. Wang, "Cognitive radio techniques under practical imperfections: a survey," *IEEE Communications Surveys & Tutorials*, vol. 17, no. 4, pp. 1858–1884, 2015.

[22] J. Song, Z. Feng, P. Zhang, and Z. Liu, "Spectrum sensing in cognitive radios based on enhanced energy detector," *IET Communications*, vol. 6, no. 8, pp. 805–809, 2012.

[23] A. Mariani, A. Giorgetti, and M. Chiani, "Effects of noise power estimation on energy detection for cognitive radio applications," *IEEE Transactions on Communications*, vol. 59, no. 12, pp. 3410–3420, 2011.

[24] M. S. Shbat and V. Tuzlukov, "Spectrum sensing under correlated antenna array using generalized detector in cognitive radio systems," *International Journal of Antennas and Propagation*, vol. 2013, Article ID 853746, 8 pages, 2013.

[25] Z. Chen, P. C. Ivanov, K. Hu, and H. E. Stanley, "Effect of nonstationarities on detrended fluctuation analysis," *Physical Review E*, vol. 65, no. 4, Article ID 041107, 2002.

[26] J. W. Kantelhardt, E. Koscielny-Bunde, H. H. A. Rego, S. Havlin, and A. Bunde, "Detecting long-range correlations with detrended fluctuation analysis," *Physica A: Statistical Mechanics and Its Applications*, vol. 295, no. 3-4, pp. 441–454, 2001.

[27] L. Xu, P. C. Ivanov, K. Hu, Z. Chen, A. Carbone, and H. E. Stanley, "Quantifying signals with power-law correlations: a comparative study of detrended fluctuation analysis and detrended moving average techniques," *Physical Review E*, vol. 71, no. 5, Article ID 051101, 2005.

[28] E. N. Lorenz, "Deterministic non periodic flow," *Journal of the Atmospheric Sciences*, vol. 20, pp. 130–141, 1963.

[29] E. Jimenez-Lopez, J. S. Gonzalez Salas, L. J. Ontanon-Garcia, E. Campos-Canton, and A. N. Pisarchik, "Generalized multistable structure via chaotic synchronization and preservation of scrolls," *Journal of the Franklin Institute*, vol. 350, no. 10, pp. 2853–2866, 2013.

[30] G. D. Durgin and T. S. Rappaport, "Effects of multipath angular spread on the spatial cross-correlation of received voltage envelopes," in *Proceedings of the IEEE VTS 49th Vehicular Technology Conference (VTC '99)*, pp. 996–1000, Houston, Tex, USA, September 1999.

[31] R. Tandra and A. Sahai, "SNR walls for signal detection," *IEEE Journal on Selected Topics in Signal Processing*, vol. 2, no. 1, pp. 4–17, 2008.

[32] M. Shbat and V. Tuzlukov, "SNR wall phenomenon alleviation using generalized detector for spectrum sensing in cognitive radio networks," *Sensors*, vol. 5, no. 7, pp. 16105–16135, 2015.